Comparison of static, dynamic, and static-dynamic eccentricity in induction machines with squirrel-cage rotors using 2D-transient FEM

Christoph Schlensok and Gerhard Henneberger
Institute of Electrical Machines (IEM), RWTH, Aachen University, Aachen, Germany

Keywords *Finite element analysis, Simulation, Inductance, Electric machines*

Abstract *Finite-element simulations of induction machines with squirrel-cage rotor require transient solution algorithms. For this reason a transient 2D solver is utilized which takes rotational movement of the rotor into account. Its formulation and the time-step algorithm are given. Two different kinds of eccentricity of the rotor and their combination are defined and studied. The three motor variants are computed and the torque, the net force, and the surface-force density are compared in time and frequency domain.*

1. Introduction

Owing to fabrication tolerances the rotors of electrical machines are usually not positioned centrically. In the case of an induction machine with squirrel-cage rotor used as a power-steering drive this has strong effect on the acoustic behavior. Eccentricity can cause extra force excitation of the stator teeth which then produces extra noise radiation. In order to estimate the effects of eccentricity the induction machine with squirrel-cage rotor is modeled and simulated using the finite-element method (FEM).

In this paper the two types of eccentricity – static and dynamic eccentricity – and their combination are simulated. Therefore, three different two-dimensional FE-models of the entire machine have to be generated. The FE-models are simulated with a 2D-transient solver which applies a node-based $\bar{A}$-approach and the first order time-step algorithm. The results provided by the solver for each time step are next to the flux-density distribution the torque and the net force acting on the rotor. Using the flux-density distribution the surface-force density is derived for each time step. Finally torque, net force and the surface-force density on the stator teeth are analyzed in time and frequency domain.

2. Definition of the different types of eccentricity

Figure 1 shows the three "pure" types of rotational movement of a rotor of an electrical machine. The centric case is the optimal case (Figure 1(a)). The rotor axis is fixed to the stator and the rotational axis. The air gap δ is equidistant along the entire circumference. Therefore, forces arising on the one side of the machine are

COMPEL: The International Journal for Computation and Mathematics in Electrical and Electronic Engineering
Vol. 23 No. 4, 2004
pp. 1070-1079

0332-1649
DOI 10.1108/03321640410553508

This article is dedicated to Prof. Gerhard Henneberger, who is released into his well deserved retirement with gratitude and appreciation for his meritorious scientific work.

compensated on the opposite in case the number of rotor slots is even. The studied machine has $N_R = 26$ rotor slots. In the case of static eccentricity which is depicted in Figure 1(b) the rotor and rotational axis are now shifted to one side of the machine. The air gap is no longer symmetrical. Owing to the fixed rotor axis the maximum and minimum force excitation are spatially fixed as well. The machine is excited very asymmetrical. If the rotational axis is then shifted back into the position of the stator axis the rotor shows dynamical eccentricity behavior (Figure 1(c)). The minimum air gap is no longer spatially fixed but rotates with the rotor as well as the maximum and minimum force excitation. Since these are "pure" types of eccentricity the most probable case is a combination of these, which is the static-dynamic case. The rotational axis lies between the rotor and the stator axis. The force excitation is a mix of both the fixed and the rotating excitation.

3. Formulations

3.1 Transient solver

The applied solver is part of the object-oriented solver package *i*MOOSE (Arians *et al.*, n.d.). The transient FEM formulation takes the rotational movement into account and two finite-element meshes have to be handled once at a time. The two-dimensional $\vec{A}$-approach is node-based. The magnetic vector potential is used in all regions. The equation

$$\int_\Gamma \left(\nabla \cdot \alpha_i \cdot \nu \cdot \nabla \cdot A_z(t) + \alpha_i \cdot \sigma \cdot \frac{\partial}{\partial t} A_z(t) \right) \mathrm{d}\Gamma = \int_\Gamma (\alpha_i \cdot J_{z0}(t)) \mathrm{d}\Gamma \tag{1}$$

has to be solved in the complete model Γ and is presented in Galerkin formulation (Arians and Henneberger, 2000). The material parameters ν and σ represent the non-linear reluctivity and the linear conductivity. The shape function of an element is defined by α_i. Triangular shaped elements are used. $J_{z0}(t)$ describes the z-component of the given coil-current density as the only excitation.

For linear interpolation of the time-dependent variables the first order time-step algorithm is applied and $A(t)$ is written as function of time:

$$A(t) = (1 - \Theta) A_n + \Theta A_{n+1} \tag{2}$$

$$\Theta = \frac{t - t_n}{t_{n+1} - t_n} = \frac{t - t_n}{\Delta t}; \quad 0 \le \Theta \le 1. \tag{3}$$

Θ is the weighting parameter and is set to $\Theta = 2/3$ according to the Galerkin scheme (Zienkiewicz and Taylor, 1989). Δt is the time step.

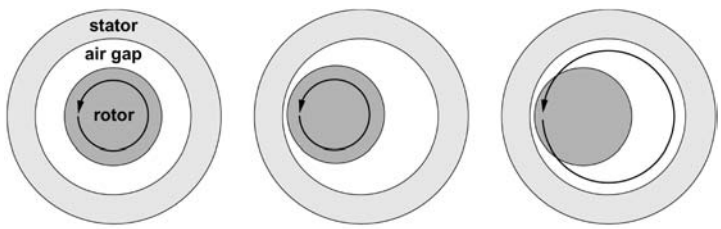

Figure 1.
Different types of eccentricity

3.2 Formulation of the surface-force density
With the Maxwell stress tensor

$$\vec{\sigma} = \frac{1}{2}\vec{n}_{12}[B_n\,(H_{1n} - H_{2n}) - (w'_1 - w'_2)] \tag{4}$$

an expression for the normal component of the local surface-force density is given (Ramesohl *et al.* (1996). The index n represents the normal components of $\vec{B}$ and H. $\vec{n}_{12}$ is the normal vector of the boundary surface from region 2 to 1. w'_1 and w'_2 are the magnetic-coenergy densities of these regions. The surface-force density vector is perpendicular to the line element. Lorentz forces and forces stemming from magnetostriction can be neglected because they are much smaller than the electro-magnetic forces.

4. Finite-element models

For the regarded application investigations have shown that an induction machine with $N_S = 36$ stator slots and $N_R = 26$ rotor bars is a very good variant. The lamination is shown in Figure 2. The machine consists of a two-layer wave-winding with three phases which is not chorded. The spread factor is $q = 3$ (Nürnberg, 1979). This results in a more sinusoidal air gap flux-density behavior. For easier modeling the two layers are not on top of each other but next to each other. This has no effect to the electromagnetic simulation because the magneto-motive force depends only on the current coverage of the slot. Since there is no symmetry in the models because of the eccentricity full 360°-models have to be generated. Figure 2 shows only the half of the model. The FE-model for the dynamic eccentric case depicted consists of $E = 13,600$ first-order triangular elements with $N = 6,874$ nodes.

In Figure 3 closeups of the maximum and minimum air gap in the initial position of the same model are depicted. The rotor is shifted $v = 0.1$ mm to the right (positive x-direction). The air gap of $\delta_{nominal} = 0.3$ mm now varies between $\delta_{min} = 0.2$ and 0.4 mm.

5. Transient 2D simulation

The three eccentric FE-models are simulated with the 2D-transient solver which calculates the torque and the net force on the rotor. The torque behavior of all three cases is shown in Figure 4.

In all three cases the torque pulsates because of the different reluctivities in each time step stemming from the rotor and stator slots. Although the average torque of

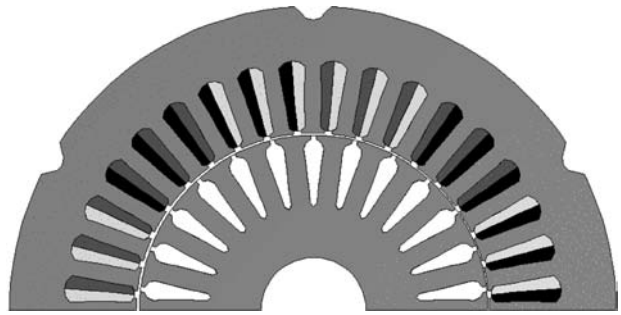

Figure 2.
Lamination of the induction machine, two pole pitches

$\overline{T} = 4.337\,\mathrm{N\,m}$ is the same for all variants the instantaneous values do not match exactly. All graphs appear to reach the maximum value at some time so it is not significant which kind of eccentricity is given.

Figure 5 shows the net-force behavior. Again the graphs of all three variants pulsate now showing a very different behavior. If the rotor is positioned statically eccentric the net force pulsates with rotor frequency:

$$f_R = 20\,\mathrm{Hz}, \quad T_R = 1/f_R = 0.05\,\mathrm{s}. \tag{5}$$

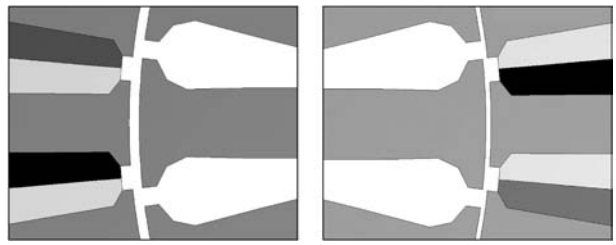

Figure 3.
Closeups of the maximum and the minimum air gap

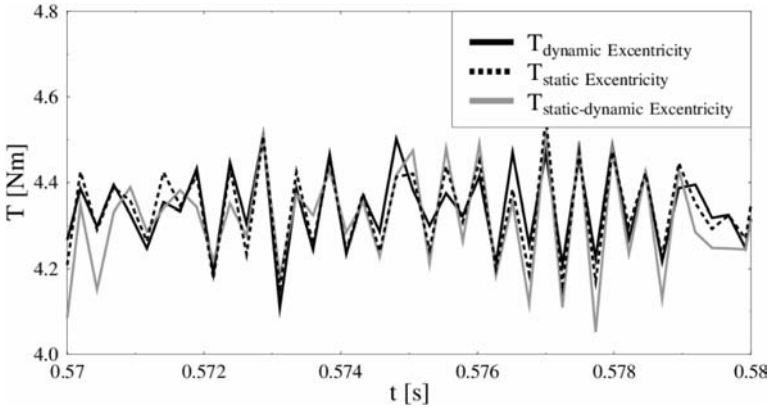

Figure 4.
Torque behavior of the three eccentric FE-models

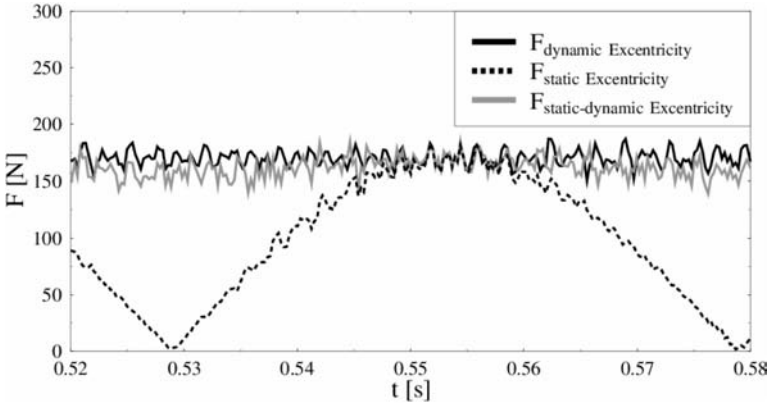

Figure 5.
Force behavior of the three eccentric FE-models

The average value in the case of static eccentricity is $\overline{F}_{stat} = 107.4\,N$. In comparison the net force in the case of dynamic eccentricity oscillates weakly. The average value is $\overline{F}_{dyn} = 170.2\,N$. When the maximum net force in the case of static eccentricity is reached the two graphs match each other. This configuration is reached for the initial position of the rotor. If both eccentricities are combined the average value is $\overline{F}_{stat-dyn} = 163.9\,N$. The net force has a main harmonic with $f_R = 20\,Hz$ because the statical portion of the signal behaves strongly like in the case of dynamic eccentricity. At the point when the maximum net force in the case of static eccentricity is reached all three graphs reach the same value. In that moment the direction of the three net forces are all the same as Figure 6 shows.

6. Computation of the excitation of the stator-teeth

The computation of the normal component, i.e. radial component, of the electromagnetic stator-teeth force-density is performed as described by Schlensok *et al.* (2003). The three computations have the same initial rotor position. The rotor is shifted in positive x-direction (to the right) with $v = 0.1\,mm$.

Figure 7 depicts the force-density distribution of the stator teeth for all three types of eccentricity for the same time step using the same scaling. In the chosen time step the rotor is positioned at $v = -0.1\,mm$ (to the left) in the case of dynamic eccentricity. The major electromagnetic force excitation is in horizontal direction. Figure 7(a) shows the distribution for dynamic eccentricity. On the left as well as on the right side the stator is assigned with about the same force values. In the case of static eccentricity which is shown in Figure 7(b) the force density has the largest values on the right side of the stator. For the combination of both types of eccentricities (Figure 7(c)) the dynamic portion outweighs the static. The maximum force density is again found on the left side although in the case of static-dynamic eccentricity the rotor is positioned in the center of the stator for this time-step. On each stator tooth itself the maximum force-density appears at the up-running edge as the zoom in Figure 7(d) depicts.

In a next step the time-dependent force-density behavior is analyzed for the up-running edge element of each stator tooth applying the Fast Fourier Transformation (FFT) (Bronstein and Semendjajew, 1991).

Figure 8 shows the spectrum that results of a FFT. The orders occurring in the spectrum are the double ($f = 96.4\,Hz$) and four times ($f = 195.7\,Hz$) the stator

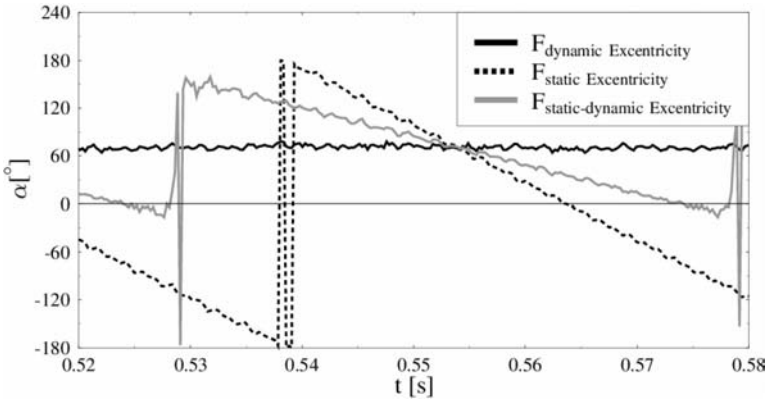

Figure 6.
Direction α of the force for all three types of eccentricity

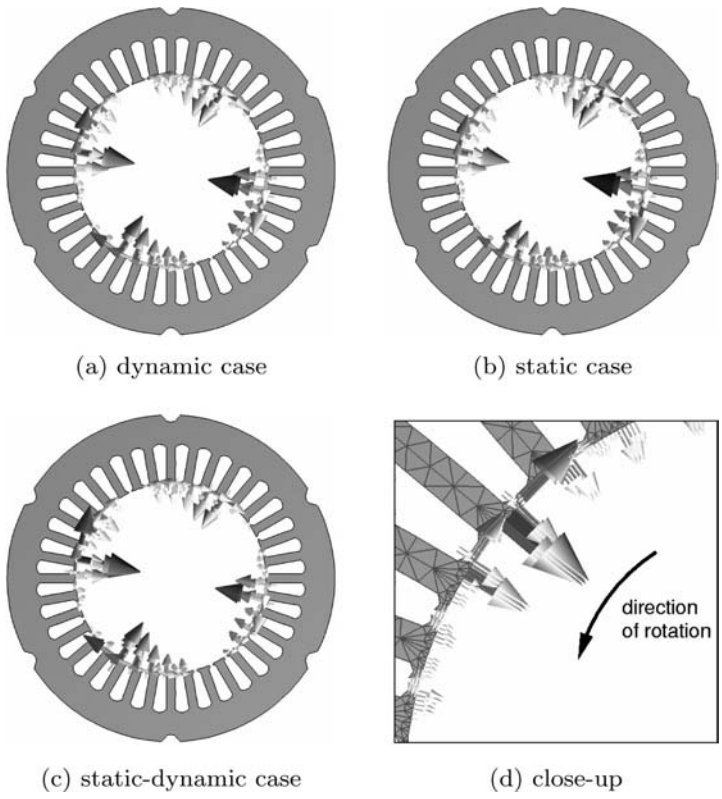

Figure 7.
Surface-force density-distribution of the stator teeth at one time step

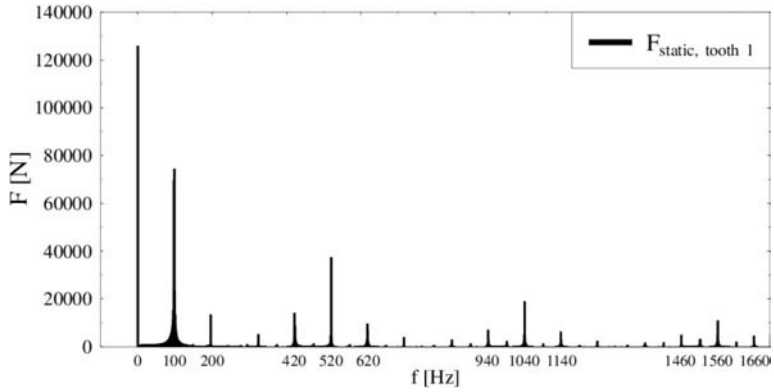

Figure 8.
Result of FFT of the force-density excitation of the element at up-running edge of stator tooth 1 for static eccentricity

frequency, the 26th ($f = 520$ Hz), 52nd ($f = 1.040$ Hz) and 78th ($f = 1.560$ Hz) order of the rotor frequency ($f_R = 20$ Hz) and their modulations with twice the stator frequency, 26th, 52nd, and 78th are the first, second, and third rotor-slot harmonics (Nau, 2000; Seinsch, 1992).

Figure 9 shows the amplitudes of the force-density of all 36 stator teeth for the first order of the rotor frequency $f_R = 20\,\text{Hz}$. The highest amplitudes are reached in the case of dynamic eccentricity. Because of the eccentric revolution of the rotor all teeth are stressed with rotor frequency in this case. For static eccentricity the effect is always stationary. So there is no interrelationship between this spectral order and the rotor frequency. If both eccentricities are combined the effects of both are mixed. So the amplitudes reach the average height of both.

For the second order of the stator frequency $f = 96.4\,\text{Hz}$ the results of the FFT are shown in Figure 10. The excitation differs depending on which tooth is regarded but is independent of the type of eccentricity. The average force density for all three calculations lies between $\sigma_{96.4\,\text{min}} = 13.4\,\text{N/m}^2$ and $\sigma_{100\,\text{max}} = 13.6\,\text{N/m}^2$. Measurements and acoustic simulations have shown that this order does not generate any significant acoustic noise although compared to the other studied orders where the highest amplitudes are reached.

Figure 11 shows that there is a strong correlation of the orders with the rotation of the rotor. The shown orders are the 26th ($f = 520\,\text{Hz}$), the 52nd ($f = 1,040\,\text{Hz}$), and the 78th ($f = 1,560\,\text{Hz}$) order of the rotor frequency ($f_R = 20\,\text{Hz}$). These are the first,

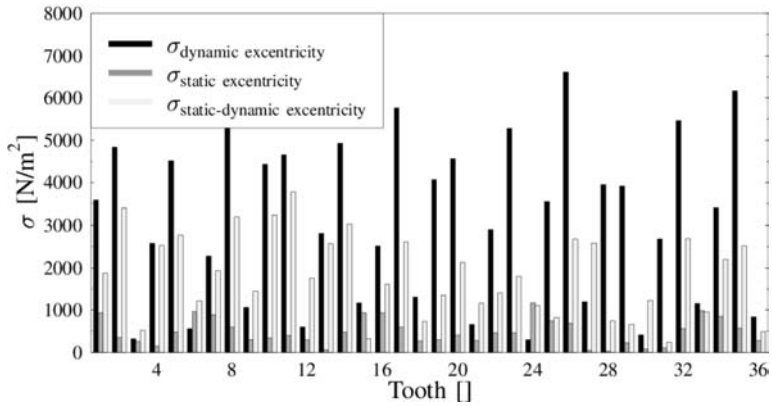

Figure 9.
Amplitudes of the force-density of all 36 stator teeth for first order of rotor frequency: $f_R = 20\,\text{Hz}$

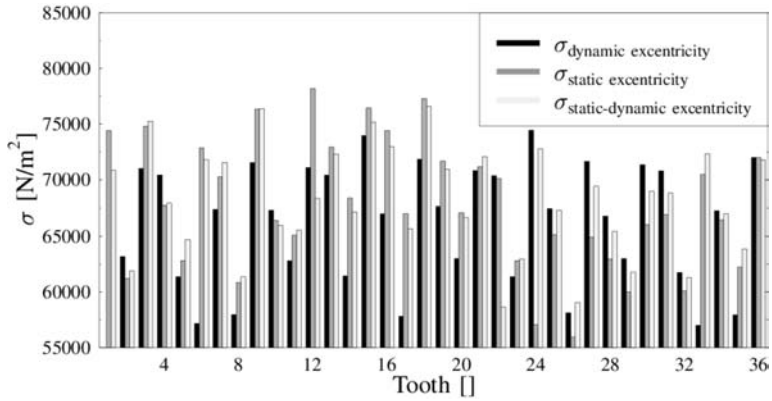

Figure 10.
Amplitudes of the force-density of all 36 stator teeth for second order of stator frequency: $f = 96.4\,\text{Hz}$

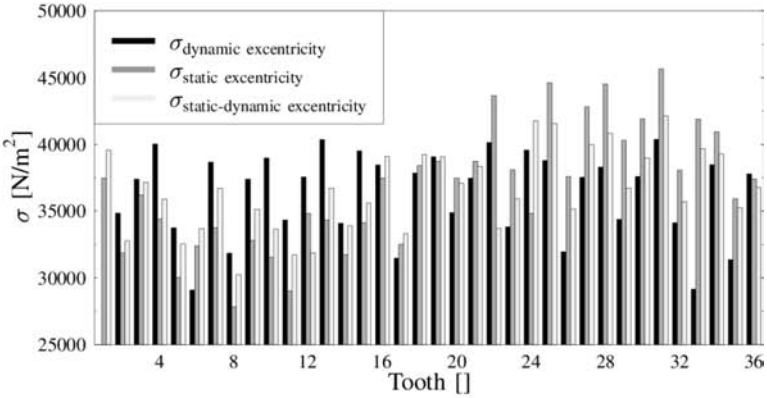

(a) $f = 520$ Hz: 26th order of rotor frequency

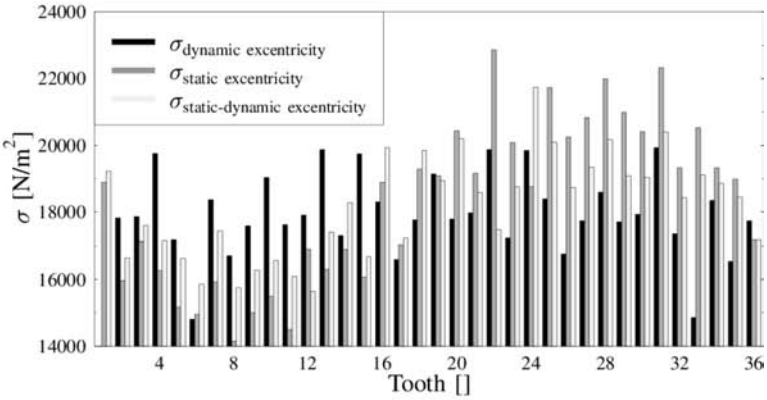

(b) $f = 1040$ Hz: 52nd order of rotor frequency

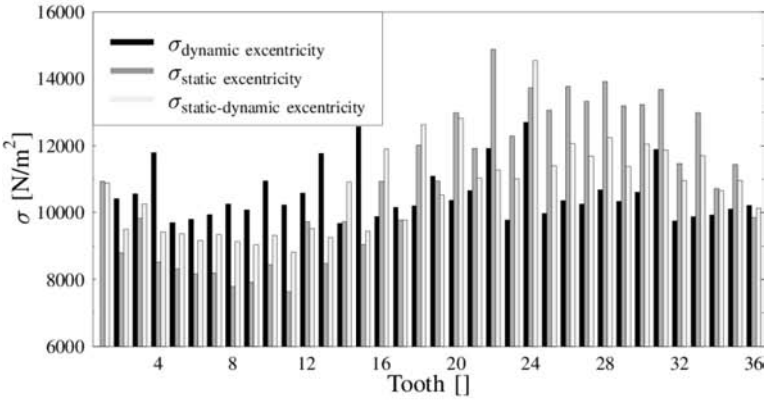

(c) $f = 1560$ Hz: 78th order of rotor frequency

Figure 11.
Amplitudes of the force density of all 36 stator teeth

second, and third rotor-slot harmonic. For all three orders the highest amplitudes for the case of static eccentricity are reached at the teeth where the air gap is smallest (near tooth 27). The lowest excitations are reached on the opposite side of the stator near tooth 9. For dynamic eccentricity all teeth are excited nearly in the same way. The amplitudes do not differ strongly. The reason is the same as in the case of $f_R = 20$ Hz. Owing to the revolving narrowest air gap the excitation revolves as well. If both cases are combined the stator teeth at the position of the smaller air gap are stressed more than those on the opposite side. Nevertheless, the effect is not as strong as in the case of static eccentricity. For all three orders shown in Figure 11 the average force density does not differ significantly depending on the type of eccentricity.

7. Conclusion

For an induction machine with squirrel-cage rotor as power-steering drive the acoustic behavior is of high significance. The subjective safety sensation of the passenger is strongly affected by the noise radiation of such important devices like the steering. Owing to the manufacturing process it is not possible to build 100 percent perfect electrical machines. This will always result in some kind of eccentricity. If the type of eccentricity which arises primarily can be detected it is possible to make predictions if there will be a strong effect on the acoustics or not.

The three types of eccentricity regarded here behave in very different ways. Dynamic eccentricity causes revolving force excitations, whereas static eccentricity produces fixed force excitations depending on the direction of the displacement of the rotor. The combination of both, the static-dynamic eccentricity, brings up both effects. Therefore, FE-models of the three variants are built and simulated with a 2D-transient solver in order to compare the effects. The formulations of the transient solver and the surface-force density are given and the time-stepping algorithm explained.

Torque and the net force acting on the rotor are computed and compared for all three models. In all three cases the torque acts in the same way and is not significantly affected by the type of eccentricity. In contrast the net-force behavior depends strongly on the case of eccentricity. For any point in time all variants are excited asymmetrically. But in the case of dynamic eccentricity the asymmetrical force excitation revolves. Static eccentricity results in fixed spatial to the direction of the minimal air gap. For the combination of both the effects are combined. The net force excitation revolves and has a stationary part as well.

In a second step the time dependent surface-force density on the stator teeth is derived from the flux-density distribution of each time step. Main orders excited are the double stator frequency and its multiples and multiples of the rotor-slot harmonics and their modulation with the double stator frequency. These orders are regarded explicitly for all 36 stator teeth and the three cases of eccentricity. Depending on the origin of the order the force density has the same amplitudes for all teeth or is fixed to the location of certain teeth. The order at double stator frequency is the same for all three variants, the order at rotor frequency is highest for the dynamic eccentricity. The other three orders (multiples of the rotor-slot harmonic) depend on the type of eccentricity and are the highest for static eccentricity and fixed to the teeth in direction of the smallest air gap. Measurements of the manufactured machines must now detect which is the most possible type of eccentricity in reality. This way the origin of the generated noise of these machines can be detected as a result of eccentricity or another source.

References

Arians, G., Bauer, T., Kaehler, C., Mai, W., Monzel, C., van Riesen, D. and Schlensok, C. (n.d.), "Innovative modern object-oriented solving environment – iMOOSE", available at: www.imoose.de

Arians, G. and Henneberger, G. (2000), "Object oriented analysis and design of transient finite element solvers applied to coupled problems", paper presented at the 9th Conference on Electromagnetic Field Computation, CEFC, Milwaukee, WI.

Bronstein, I.N. and Semendjajew, K.A. (1991) in Teubner, B.G. (Ed.), *Taschenbuch der Mathematik, 25. Auflage*, Verlagsgesellschaft, Stuttgart, Leipzig.

Nau, S.L. (2000), "Acoustic noise of induction electric motor: causes and solutions", paper presented at the Second International Seminar on Vibrations and Acoustic Noise of Electric Machinery, Lódź, September, VANEM.

Nürnberg, W. (1979), *Die Asynchronmaschine*, Springer, Berlin, Göttingen, Heidelberg.

Ramesohl, I., Küppers, S., Hadrys, W. and Henneberger, G. (1996), "Three dimensional calculation of magnetic forces and displacements of a claw-pole generator", *IEEE Transactions on Magnetics*, Vol. 32 No. 3, pp. 1685-8.

Schlensok, C., Schneeloch, G. and Henneberger, G. (2003), "Analysis of stator-teeth forces in induction machines with squirrel cages using 2D-FEM", paper presented at the 6th International Symposium on Electric and Magnetic Fields, EMF, Aachen.

Seinsch, H.O. (1992), in Teubner, B.G. (Ed.), *Oberfelderscheinungen in Drehfeldmaschinen*, Stuttgart.

Zienkiewicz, O.C. and Taylor, R.L. (1989), *The Finite Element Method*, McGraw-Hill Book Company, London, pp. 346-61.